JOURNAL OF ENZYME INHIBITION AND MEDICINAL CHEMISTRY, 2017
VOL. 32, NO. 1, 20–28
http://dx.doi.org/10.1080/14756366.2016.1230109

Taylor & Francis
Taylor & Francis Group

RESEARCH ARTICLE

OPEN ACCESS

# Diethylalkylsulfonamido(4-methoxyphenyl)methyl)phosphonate/phosphonic acid derivatives act as acid phosphatase inhibitors: synthesis accompanied by experimental and molecular modeling assessments

Nahid Alimoradi[a]*, Mohammad Reza Ashrafi-Kooshk[b]*, Mohsen Shahlaei[c], Shabnam Maghsoudi[b], Hadi Adibi[d], Ross P. McGeary[e] and Reza Khodarahmi[b]

[a]Student Research Committee, Kermanshah University of Medical Sciences, Kermanshah, Iran; [b]Medical Biology Research Center, Kermanshah University of Medical Sciences, Kermanshah, Iran; [c]Nano Drug Delivery Research Center, Kermanshah University of Medical Sciences, Kermanshah, Iran; [d]Pharmaceutical Sciences Research Center, Faculty of Pharmacy, Kermanshah University of Medical Sciences, Kermanshah, Iran; [e]The University of Queensland, School of Chemistry and Molecular Biosciences, St. Lucia, QLD, Australia

**ABSTRACT**

Purple acid phosphatases (PAPs) are binuclear metallo-hydrolases that have been isolated from various mammals, plants, fungi and bacteria. In mammals, PAP activity is associated with bone resorption and can lead to bone metabolic disorders such as osteoporosis; thus human PAP is an attractive target to develop anti-osteoporotic drugs. The aim of the present study was to investigate inhibitory effect of synthesized diethylalkylsulfonamido(4-methoxyphenyl)methyl)phosphonate/phosphonic acid derivatives as potential red kidney bean PAP (rkbPAP) inhibitors accompanied by experimental and molecular modeling assessments. Enzyme kinetic data showed that they are good rkbPAP inhibitors whose potencies improve with increasing alkyl chain length. Hexadecyl derivatives, as most potent compounds ($K_i = 1.1\ \mu M$), inhibit rkbPAP in the mixed manner, while dodecyl derivatives act as efficient noncompetitive inhibitor. Also, analysis by molecular modeling of the structure of the rkbPAP–inhibitor complexes reveals factors, which may be important for the determination of inhibition specificity.

**ARTICLE HISTORY**
Received 25 March 2016
Revised 16 July 2016
Accepted 18 August 2016

**KEYWORDS**
Acid phosphatase; enzyme inhibition; phosphonic acid; synthesis

## Introduction

Purple acid phosphatase (PAP; E.C.3.1.3.2) is a binuclear hydrolase that has been isolated from various mammals and plants[1]. Mammalian PAP is also known as tartrate-resistant acid phosphatase[2] or osteoclastic acid phosphatase[3]. These enzymes are distinguished from other acid phosphatases by their characteristic purple color in concentrated solution[4]. PAPs catalyze the hydrolysis of phosphorylated substrates under neutral to acidic conditions *in vivo*[1]. Several crystal structures of PAPs have been described, including those from plants (red kidney bean and a sweet potato PAP) as well as from mammals (pig, human and rat)[5] and references 90–93 therein. The enzyme structures from the two plant organisms are homodimers consisting of 55 kDa subunits, while the mammalian PAPs are 35 kDa monomers[6–9]. Despite the apparent difference between the structures of plant and animal PAPs, and the low degree of overall amino acid sequence homology between enzymes from different kingdoms, their catalytic sites display a remarkable similarity[5] and references 2, 89, 107 therein (Figure 1) and include two metal centers, which are coordinated by seven invariant ligands (one aspartate, one tyrosine and one histidine for $Fe^{3+}$ and two histidines and one asparagine for $Zn^{2+}$), with an aspartate residue bridging the two ions[10]. Due to the structural similarity in their catalytically relevant active sites, all PAPs are believed to employ highly conserved mechanistic strategies[1].

The biological roles of PAPs are diverse and depend on the host organism. Plant PAPs are believed to assist in mobilizing organic phosphate esters in soil during germination[11], and mammalian PAPs have been linked with iron transport during pregnancy[12]. Both may be involved in bacterial killing since they are able, at least *in vitro*, to generate reactive oxygen species via Fenton chemistry as a response against pathogens[9,13,14]. The association of mammalian PAP activity with osteoporosis[2,15–17] has prompted investigators, around the world, to examine its potential as a therapeutic target for the treatment of this disease, and to develop potent inhibitors of this enzyme[17,18]. It is known that PAP is secreted into the bone-resorptive space in mammals[2], and PAP activity has long been associated with bone resorption[19]. In addition, transgenic mice in which the PAP enzyme was over-expressed developed osteoporosis due to increased bone resorption[20], whereas the corresponding knockout mice exhibited the opposite condition (osteopetrosis), further implicating the role of PAP in this process[4], and establishing PAP as a drug target in the treatment of osteoporosis[21]. Although clinical treatments are available for osteoporosis, notably bisphophonates, which inhibit farnesylpyrophosphate synthase in osteoclast[22], but these drugs have significant side effects and compliance issues. Also, a number of PAPs inhibitors including fluoride[23], and several tetrahedral inorganic oxyanions, including phosphate, arsenate, vanadate, tungstate and molybdate[7,24] have been discovered, but most of

**CONTACT** Hadi Adibi hadibi@kums.ac.ir Pharmaceutical Sciences Research Center, Faculty of Pharmacy, Kermanshah University of Medical Sciences, Kermanshah, Iran; Reza Khodarahmi rkhodarahmi@kums.ac.ir, rkhodarahmi@mbrc.ac.ir Medical Biology Research Center, Kermanshah University of Medical Sciences, Kermanshah, Iran
*These authors had equally contributed.

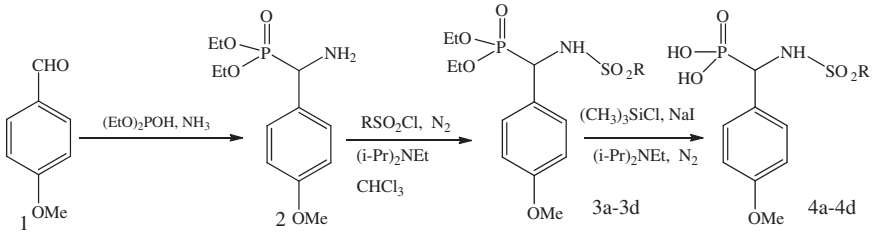


3a,4a: R= *n*-Hexyl, 3b,4b: *n*-Octyl, 3c,4c: *n*-Dodecyl, 3d,4d: *n*-Hexadecyl

**Scheme 1.** Synthesis of diethylalkylsulfonamido(4-methoxyphenyl)methyl)phosphonate/phosphonic acid derivatives.

these do not possess drug-like properties and so are not suitable for further modifications that may convert them into chemotherapeutic agents. Myers et al.[25] have described a number of simple phosphonates with pendant metal-binding groups, such as thiol, phosphonate and carboxylate, and these have shown inhibitory activity against red kidney PAP (rkbPAP), in the range 80–3000 μM. Moreover, several modified phosphotyrosine containing tripeptides have also shown inhibitory activity toward several mammalian and plant PAPs, with $IC_{50}$ values in the mid-micromolar range[21]. More recently, α-alkoxynaphthylmethylphosphonic acids and acyl derivatives of α-aminonaphthylmethylphosphonic acid have also been shown to be PAP inhibitors with $K_i$ and $IC_{50}$ values in the low micromolar range[18,26]. These molecules were designed as the derivatives of 1-naphthylmethylphosphonic acid, a PAP inhibitor previously reported by Schwender et al.[3] A number of phosphonate- and carboxylate-containing derivatives of these substrates have been synthesized, and these displayed mid- to low-micromolar inhibitory potency against several mammalian and plant PAPs[21].

The current study is particularly novel and significant because to the best of our knowledge, no previous similar studies have been reported on possible inhibitory potential of diethylalkylsulfonamido(4-methoxyphenyl)methyl)phosphonate/phosphonic acid derivatives on the PAP enzyme. Based on previous lead compound(s) and rational drug design, different sulfonyl derivatives of alkylsulfonamido(4-methoxyphenyl)methyl)phosphonic acid with varying lengths of alkyl chains were synthesized and evaluated as PAP inhibitors. The sulfonyl and alkyl groups were introduced for two reasons: (i) the sulfonyl group was expected to improve the water solubility of these compounds; (ii) McGeary et al. have previously reported that PAP inhibitors bearing an alkoxy group with long alkyl chain were superior to those that did not, suggesting effective hydrophobic interactions between the alkyl group of the inhibitors and nonpolar surface residue near the enzyme's active site[18]; (iii) a nonclassical bioisosteric replacement was made in which the acyl moiety was changed to sulfonamide one. Therefore, inhibitors of general structures in Scheme 1 with $C_6$, $C_8$, $C_{12}$ and $C_{16}$ alkyl chains were examined. Moreover, to evaluation of coordination of phosphonate moiety to the bimetal center, the ethyl groups were attached to the oxygen atoms of phosphonate. The aim of the current study was also to expand this working framework through suggesting a molecular modeling component to advance the mechanistic understanding of PAP–drug interactions.

## Materials and methods

### Chemistry

All starting materials, reagents, and solvents were purchased from Merck Finnigan (Germany). The purity of the synthesized compounds was confirmed by thin layer chromatography (TLC) using various solvents of different polarities. Merck silica gel 60 F254 plates were applied for analytical TLC. Column chromatography was performed on Merck silica gel (70–230 mesh) for purification of the intermediate and final compounds. Melting points were determined on a Kofler hot stage apparatus (Vienna, Austria) and are uncorrected. $^1$H NMR spectra were recorded using a Bruker 500 spectrometer (Bruker, Rheinstatten, Germany), and chemical shifts are expressed as $\delta$ (ppm) with tetramethylsilane (TMS) as an internal standard. Coupling constants (*J*) are reported in hertz and peak multiplicities described as singlet (s), doublet (d), triplet (t), multiplet (m) or broad (br). The IR spectra were obtained on a Shimadzu 470 (Shimadzu, Tokyo, Japan) spectrophotometer (potassium bromide disks). The mass spectra were run on a Finnigan TSQ-70 spectrometer (Finnigan) at 70 eV.

### General procedure for the syntheses and spectral data of the synthesized compounds

#### General procedure for the synthesis of diethyl(amino(4-methoxyphenyl)methyl)phosphonate (2)

This compound was prepared according to the general procedure described in the literature[3,18,26,27]. $NH_4OAc$ (7.70 g, 0.10 mol) was added to EtOH (20 mL) in the round-bottomed flask containing the activated molecular sieves, followed by the addition of *p*-methoxybenzaldehyde (**1**) (13.60 mL, 0.10 mol) and diethyl phosphite (12.90 mL, 0.10 mol). The reaction mixture was stirred at 60 °C under nitrogen atmosphere for 48 h. Once it has cooled to room temperature, conc. HCl was added to the resulting mixture to acidify it to pH 1, and then was washed with $Et_2O$ (50 mL). Addition of 2 M NaOH to the aqueous layer changed the pH to 11, and the product was extracted with dichloromethane (100 mL) to give the free base of diethyl (amino(naphthalen-1-yl)methyl)phosphonate[27] as yellow oil. The product was later treated with HCl gas in EtOH (10 mL)–$Et_2O$ (10 mL). $Et_2O$ (20 mL) was further added to the resulting solution, and the solvent was evaporated to obtain the hydrochloride salt of diethyl compound **2** as white solid.

#### General procedure for the preparation of diethyl (alkylamido(4-methoxyphenyl)methyl)phosphonates (3a–3d)

This compound was prepared according to the general procedure described in the literature[27]. A solution of DIPEA (2.60 mL, 15.2 mmol) and the hydrochloride salt **2** (0.50 g, 1.52 mmol) in $CH_2Cl_2$ (5 mL) were then added dropwise to the sulfonyl chloride and the reaction mixture was stirred under argon $N_2$ for 24 h. The crude product was purified using silica flash column chromatography (10–60% EtOAc in light petroleum) to give **3a**–**3h**.

#### General procedure for the preparation of (alkylamido(4-methoxyphenyl)methyl)phosphonic acids (4a–4d)

This compound was prepared according to the general procedure described in the literature[27]. NaI (5 equiv) and distilled MeCN

(5 mL) were added to the corresponding diethyl ester **3a**–**3d** (1 equiv). Distilled TMSCl (5 equiv) was then added to the mixture, which was then stirred at 40 °C under $N_2$ for 18 h. MeCN was removed *in vacuo*. The precipitate was then extracted with EtOAc (3 × 10 mL), washed with $NaS_2O_3$ (10 mL), water and NaCl (2 × 10 mL), followed by drying with $NaSO_4$. The product was then co-evaporated with toluene (3 × 5 mL), and purified under high vacuum to give the corresponding phosphonic acids **4a**–**4d**.

### *Diethyl(amino(4-methoxyphenyl)methyl)phosphonate (2)*

*Molecular weight*: 204 (g/mol), FT-IR (KBr, $cm^{-1}$): 3429 (stretch NH), 2935 (stretch CH, aromatic), 2904 (stretch CH, aliphatic), 1608 (stretch C=C, aromatic), 1519 (bending NH), 1462 (bending $CH_2$), 1388 (bending $CH_3$), 1242 (stretch C–O), 1026 (stretch C–O, $OCH_3$), 948 (stretch CH, oop), 547 (bending NH).

### *Diethyl(hexylsulfonamido(4-methoxyphenyl)methyl)phosphonate (3a)*

*Molecular weight*: 421 (g/mol), FT-IR (KBr, $cm^{-1}$): 3437 (stretch NH), 2931 (stretch CH, aromatic), 2873 (stretch CH, aliphatic), 1612 (stretch C=C, aromatic), 1516 (bending NH), 1465 (bending $CH_2$), 1392 (bending $CH_3$), 1311, 1188 (stretch O=S=O), 1249 (stretch C–O), 1041 (stretch C–O, $OCH_3$), 952 (stretch CH, oop), 551 (bending NH).

$^1$H NMR ($CDCl_3$, 300 MHz): $\delta$ (ppm): 7.68–7.66 (d, $J$ = 6 Hz, 1H, N**H**), 7.39–7.36 (dd, $J$ = 1.5, 1.5 Hz, 2H, $C_{(2,6)}$**H** aromatic), 6.80–6.78 (d, $J$ = 6.6 Hz, 2H, $C_{(3,5)}$**H** aromatic), 5.52–5.44 (dd, $J$ = 7.2, 7.2 Hz, H, C**H**–P), 4.15–4.04 (m, 2H, $C_{(1,1*)}$**H**–OP), 3.88–3.79 (m, 1H, $C_{(1)}$**H**–OP), 3.72 (s, 3H, C**H$_3$**–O), (m, 1H, $C_{(1*)}$**H**–OP), 2.16 (t, $J$ = 5.7 Hz, 2H, C**H$_2$**–S), 1.53 (t, $J$ = 5.4 Hz, 2H, C**H$_2$**–$CH_2$S), 1.28 (t, $J$ = 5.4 Hz, 3H, $C_{(2)}$**H$_3$**–$CH_2$O), 1.15 (bro, $J$ = 7.5 Hz, 10H, C**H** aliphatic), 1.03 (t, $J$ = 5.7 Hz, 3H, $C_{(2*)}$**H$_3$**–$CH_2$O), 0.80 (t, $J$ = 5.4 Hz, 3H, C**H$_3$**–RS).

### *Diethyl((4-methoxyphenyl)(octylsulfonamido)methyl)phosphonate (3b)*

*Molecular weight*: 449 (g/mol), FT-IR (KBr, $cm^{-1}$): 3437 (stretch NH), 2927 (stretch CH, aromatic), 2858 (stretch CH, aliphatic), 1612 (stretch C=C, aromatic), 1512 (bending NH), 1465 (bending $CH_2$), 1396 (bending $CH_3$), 1303, 1215 (stretch O=S=O), 1246 (stretch C–O), 1037(stretch C–O, $OCH_3$), 948(stretch CH, oop), 721 (rocking $CH_2$), 551 (bending NH).

$^1$H NMR ($CDCl_3$, 300 MHz): $\delta$ (ppm): 7.54–7.49 (dd, $J$ = 3.6, 3.6 Hz, 1H, N**H**), 7.39–7.35 (dd, $J$ = 2.1, 2.1 Hz, 2H, $C_{(2,6)}$**H** aromatic), 6.81–6.78 (dd, $J$ = 9 Hz, 2H, $C_{(3,5)}$**H** aromatic), 5.53–5.46 (dd, $J$ = 20.7 Hz, H, C**H**–P), 4.14–4.04 (m, 2H, $C_{(1,1*)}$**H**–OP), 3.88–3.80 (m, 1H, $C_{(1)}$**H**–OP), 3.73 (s, 3H, C**H$_3$**–O), 3.68–3.59 (m, 1H, $C_{(1*)}$**H**–OP), 2.17 (t, $J$ = 7.8 Hz, 2H, C**H$_2$**–S), 1.54 (t, $J$ = 6.9 Hz, 2H, C**H$_2$**–$CH_2$S), 1.28 (t, $J$ = 7.2 Hz, 3H, $C_{(2)}$**H$_3$**–$CH_2$O), 1.16 (bro, $J$ = 7.5 Hz, 10H, C**H** aliphatic), 1.04 (t, $J$ = 7.2 Hz, 3H, $C_{(2*)}$**H$_3$**-$CH_2$O), 0.81 (t, $J$ = 6.9 Hz, 3H, C**H$_3$**–RS).

$^{13}$C NMR ($CDCl_3$, 75 MHz): $\delta$ (ppm): 13.9 (CH3–RS), 16.1 ($C_{(2*)}$H3 ethoxy), 16.3 ($C_{(2)}$H3 ethoxy), 22.5 & 22.6 & 29.1 & 29.2 & 31.7 & 36.1 ($CH_2$ alkyl), 48.1($C_{(1*)}H_2$ ethoxy), 49.7 ($C_{(1)}H_2$ ethoxy), 55.0 (P–CH–N), 62.8 (S–$CH_2$), 63.1 ($CH_3$ methoxy), 113.7 ($C_{3,5}$ phenyl), 127.3 ($C_{2,6}$ phenyl), 129.4 ($C_1$ phenyl), 159.2 ($C_4$ phenyl).

### *Diethyl(dodecylsulfonamido(4-methoxyphenyl)methyl)phosphonate (3c)*

*Molecular weight*: 505 (g/mol), FT-IR (KBr, $cm^{-1}$): 3444 (stretch NH), 2924 (stretch CH, aromatic), 2854 (stretch CH, aliphatic), 1651 (stretch C=C, aromatic), 1512 (bending NH), 1458 (bending $CH_2$), 1396 (bending $CH_3$), 1311, 1176 (stretch O=S=O), 1211(stretch C–O), 1041 (stretch C–O, $OCH_3$), 948 (stretch CH, oop), 729 (rocking $CH_2$), 547 (bending NH).

$^1$H NMR ($CDCl_3$, 300 MHz): $\delta$ (ppm): 7.55–7.53 (dd, $J$ = 2.1, 2.1 Hz, 1H, N**H**), 7.38–7.36 (dd, $J$ = 1.2 Hz, 2H, $C_{(2,6)}$**H** aromatic), 6.81–6.79 (d, $J$ = 5.1 Hz, 2H, $C_{(3,5)}$**H** aromatic), 5.51–5.45 (dd, $J$ = 5.7, 5.7 Hz, H, C**H**–P), 4.13–4.07 (m, 2H, $C_{(1,1*)}$**H**–OP), 3.85–3.82 (m, 1H, $C_{(1)}$**H**–OP), 3.73 (s, 3H, C**H$_3$**–O), 3.66–3.61 (m, 1H, $C_{(1*)}$**H**–OP), 2.17 (t, $J$ = 4.2 Hz, 2H, C**H$_2$**–S), 1.54 (t, $J$ = 6.9 Hz, 2H, C**H$_2$**–$CH_2$S), 1.28 (t, $J$ = 4.2 Hz, 3H, $C_{(2)}$**H$_3$**–$CH_2$O), 1.16 (bro, $J$ = 7.5 Hz, 10H, C**H** aliphatic), 1.04 (t, $J$ = 4.2 Hz, 3H, $C_{(2*)}$**H$_3$**–$CH_2$O), 0.83 (t, $J$ = 6.9 Hz, 3H, C**H$_3$**–RS).

$^{13}$C NMR ($CDCl_3$, 75 MHz): $\delta$ (ppm): 13.9 (CH3–RS), 16.1 ($C_{(2*)}$H3 ethoxy), 16.3 ($C_{(2)}$H3 ethoxy), 22.5 & 22.6 & 29.1 & 29.2 & 29.4 & 31.7 & 36.2 ($CH_2$ alkyl), 48.4($C_{(1*)}H_2$ ethoxy), 49.6 ($C_{(1)}H_2$ ethoxy), 55.1 (P–CH–N), 62.8 (S–$CH_2$), 63.1 ($CH_3$ methoxy), 113.8 ($C_{3,5}$ phenyl), 127.3 ($C_{2,6}$ phenyl), 129.4 ($C_1$ phenyl), 159.2 ($C_4$ phenyl).

### *Diethyl(hexadecylsulfonamido(4-methoxyphenyl)methyl)phosphonate (3d)*

*Molecular weight*: 561 (g/mol), FT-IR (KBr, $cm^{-1}$): 3433 (stretch NH), 2920 (stretch CH, aromatic), 2850 (stretch CH, aliphatic), 1608 (stretch C=C, aromatic), 1512 (bending NH), 1465 (bending $CH_2$), 1400 (bending $CH_3$), 1307, 1184 (stretch O=S=O), 1249 (stretch C–O), 1053 (stretch C–O, $OCH_3$), 968 (stretch CH, oop), 721 (rocking $CH_2$), 536 (bending NH).

$^1$H NMR ($CDCl_3$, 300 MHz): $\delta$ (ppm): 7.36–7.33 (dd, $J$ = 1.5, 1.8 Hz, 2H, $C_{(2,6)}$**H** aromatic), 6.85–6.83 (d, $J$ = 6.3 Hz, 2H, $C_{(3,5)}$**H** aromatic), 6.60–6.56 (dd, $J$ = 3.3, 3.3 Hz, 1H, N**H**), 5.47–5.40 (dd, $J$ = 7.2, 7.2 Hz, H, C**H**–P),4.13–4.07 (m, 2H, $C_{(1,1*)}$**H**–OP), 3.92–3.86 (m, 1H, $C_{(1)}$**H**–OP), 3.70 (s, 3H, C**H$_3$**–O), 3.68–3.64 (m, 1H, $C_{(1*)}$**H**–OP), 2.19 (t, $J$ = 6 Hz, 2H, C**H$_2$**–S), 1.58 (t, $J$ = 5.7 Hz, 2H, C**H$_2$**–$CH_2$S), 1.29 (t, $J$ = 5.1 Hz, 3H, $C_{(2)}$**H$_3$**–$CH_2$O), 1.23 (bro, $J$ = 7.5 Hz, 26H, C**H** aliphatic), 1.07 (m, $J$ = 5.1 Hz, 3H, $C_{(2*)}$**H$_3$**–$CH_2$O), 0.85 (t, $J$ = 5.4 Hz, 3H, C**H$_3$**–RS).

### *(Hexylsulfonamido(4-methoxyphenyl)methyl)phosphonic acid (4a)*

*Molecular weight*: 365 (g/mol), FT-IR (KBr, $cm^{-1}$): 3433 (stretch NH), 2931 (stretch CH, aromatic), 2866 (stretch CH, aliphatic), 1612 (stretch C=C, aromatic), 1516 (bending NH), 1462 (bending $CH_2$), 1392 (bending $CH_3$), 1303, 1188 (stretch O=S=O), 1045 (stretch C–O, $OCH_3$), 952 (stretch CH, oop), 775 (rocking $CH_2$), 559 (bending NH).

$^1$H NMR ($CH_3OH$-$d_4$, 300 MHz): $\delta$ (ppm): 7.38–7.35 (d, $J$ = 8.4 Hz, 2H, $C_{(2,6)}$**H** aromatic), 6.90–6.86 (d, $J$ = 4.2 Hz, 2H, $C_{(3,5)}$**H** aromatic), 5.46–5.29 (dd, $J$ = 21, 21 Hz, H, C**H**-P), 3.77 (s, 3H, C**H$_3$**–O), 2.28 (t, $J$ = 7.2 Hz, 2H, C**H$_2$**–S), 1.59 (t, $J$ = 5.7 Hz, 2H, C**H$_2$**–$CH_2$S), 1.25 (bro, 6H, C**H** aliphatic), 0.85 (t, $J$ = 5.4 Hz, 3H, C**H$_3$**–RS).

MS (*m/z*, %): 365 (M), 364 (M-1, 4), 336 (M-29, 1), 310(M-57, 2), 284 (M-81, 9), 216 (M-148, 2), 163 (M-201, 18), 148 (M-216, 11), 136 (M-229, 26), 106 (M-259, 9), 91 (M-274, 13), 83 (M-282, 49), 72 (M-293, 78), 56 (M-311, 76), 43 (M-292, 97).

### *((4-Methoxyphenyl)(octylsulfonamido)methyl)phosphonic acid (4b)*

*Molecular weight*: 393 (g/mol), FT-IR (KBr, $cm^{-1}$): 3606 (stretch NH), 2927 (stretch CH, aromatic), 2858 (stretch CH, aliphatic), 1612 (stretch C=C, aromatic), 1516 (bending NH), 1462 (bending $CH_2$), 1396 (bending $CH_3$), 1307, 1184 (stretch O=S=O), 1041 (stretch

C–O, $OCH_3$), 960 (stretch CH, oop), 729 (rocking $CH_2$), 547 (bending NH).

$^1$H NMR ($CH_3OH$-$d_4$, 300 MHz): $\delta$ (ppm): 7.38–7.36 (dd, $J = 1.2$ Hz, 2H, $C_{(2,6)}$**H** aromatic), 6.9–6.87 (dd, $J = 6.6$ Hz, 2H, $C_{(3,5)}$**H** aromatic), 5.45–5.30 (dd, $J = 15.9$, 5.9 Hz, H, C**H**–P), 3.76 (s, 3H, C**H$_3$**–O), 2.29–2.26 (m, 2H, C**H$_2$**–S), 1.59 (t, $J = 5.1$ Hz, 2H, C**H$_2$**–$CH_2$S), 1.25 (bro, 10H, C**H** aliphatic), 0.88 (t, $J = 2.4$ Hz, 3H, C**H$_3$**–RS).

MS (*m/z*, %): 393 (M), 321 (M-71, 12), 313 (M-80, 39), 299 (M-94, 17), 204 (M-189, 5), 176 (M-217, 19), 164 (M-229, 18), 148 (M-245, 25), 135 (M-258, 100).

### *(Dodecylsulfonamido(4-methoxyphenyl)methyl)phosphonic acid (4c)*

*Molecular weight*: 449 (g/mol), FT-IR (KBr, $cm^{-1}$): 3410 (stretch NH), 2920 (stretch CH, aromatic), 2850 (stretch CH, aliphatic), 1612 (stretch C=C, aromatic), 1512 (bending NH), 1462 (bending $CH_2$), 1392 (bending $CH_3$), 1307, 1184 (stretch O=S=O), 1053 (stretch C–O, $OCH_3$), 952 (stretch CH, oop), 725 (rocking $CH_2$), 559 (bending NH).

$^1$H NMR ($CH_3OH$-$d_4$, 300 MHz): $\delta$ (ppm): 7.37–7.36 (dd, $J = 4.8$ Hz, 2H, $C_{(2,6)}$**H** aromatic), 6.88 (t, $J = 5.1$ Hz, 2H, $C_{(3,5)}$**H** aromatic), 5.45–5.31 (dd, $J = 12.51$, 12.57 Hz, H, C**H**–P), 3.76 (s, 3H, C**H$_3$**–O), 2.27 (t, $J = 1.8$ Hz, 2H, C**H$_2$**–S), 1.58 (t, $J = 5.7$ Hz, 2H, C**H$_2$**–$CH_2$S), 1.25 (bro, 18H, C**H** aliphatic), 0.88 (t, $J = 5.4$ Hz, 3H, C**H$_3$**–RS).

MS (*m/z*, %): 450 (M + 1), 368(M − 81, 25), 281 (M − 169, 12), 233 (M − 217, 17), 218 (M − 232, 13), 163 (M − 286, 33), 148 (M-301, 40), 135 (M − 314, 100).

### *(Hexadecylsulfonamido(4-methoxyphenyl)methyl)phosphonic acid (4d)*

*Molecular weight*: 505 (g/mol), FT-IR (KBr, $cm^{-1}$): 3603 (stretch OH), 3356 (stretch NH), 2916 (stretch CH, aromatic), 2850 (stretch CH, aliphatic), 1612 (stretch C=C, aromatic), 1512 (bending NH), 1465 (bending $CH_2$), 1392 (bending $CH_3$), 1311, 1180 (stretch O=S=O), 1037 (stretch C–O, $OCH_3$), 952 (stretch CH, oop), 721 (rocking $CH_2$), 555 (bending NH).

$^1$H NMR ($CH_3OH$-$d_4$, 300 MHz): $\delta$ (ppm): 7.36–7.34 (d, $J = 4.8$ Hz, 2H, $C_{(2,6)}$**H** aromatic), 6.86–6.84 (d, $J = 4.8$ Hz, 2H, $C_{(3,5)}$**H** aromatic), 3.74 (s, 3H, C**H$_3$**–O), 2.27 (s, 2H, C**H$_2$**–S), 1.57 (s, 2H, C**H$_2$**–$CH_2$S), 1.25 (s, Hz, 26H, C**H** aliphatic), 0.86 (t, $J = 5.4$ Hz, 3H, C**H$_3$**–RS).

MS (*m/z*, %): 505 (M), 425 (M − 80, 27), 338 (M − 167, 2), 316 (M − 189, 12), 302 (M − 203, 17), 289 (M − 217, 9), 282 (M − 223, 6), 224 (M − 281, 77), 212 (M − 293, 8), 204 (M − 301, 25), 190 (M − 315, 100).

### Enzyme preparation and purification

PAP from red kidney bean (rkbPAP) was purified following a previously published protocol[8]. Briefly, red kidney beans (*Phaseolus vulgaris*), provided from local market, were ground and suspended in 0.5 M sodium chloride solution. The suspension was filtered through a muslin cloth, followed by ethanol fractionation and ammonium sulfate precipitation. The purple enzyme solution was dialyzed against several changes of 0.25 M NaCl over a period of several days. The purple precipitate, which formed in the dialysis bag was collected by centrifugation. The resulting preparation stored at 4 °C in 0.5 M NaCl. The protein identity and purity was tested by SDS–polyacrylamide gel electrophoresis (SDS–PAGE) and by comparing with molecular weight protein markers, by loading the protein samples on a 12% slab gel. Protein concentration was determined by Lowry method[28].

### Enzyme assay

Inhibition assays for rkbPAP was performed in 96-well multi-titer plates using a microplate reader. Kinetic measurements were taken at pH 4.9 (0.1 M sodium citrate buffer with 5% DMSO) at 25 °C using *p*-nitrophenyl phosphate (*p*-NPP) as the substrate at concentrations of 1, 2, 4, 6, 8, 10, 12, 14, 18 and 24 mM[29]. The hydrolysis of *p*-NPP by PAP produces *p*-nitrophenol (*p*-NP), which has a characteristic intense yellow color at 405 nm with $\varepsilon = 343$ $M^{-1}$ $cm^{-1}$ [18,26]. The concentration of enzyme used was ~60 nM, while at least eight concentrations of each compound ranged from 50 to 2000 μM. The $IC_{50}$ values obtained by "Dose–response inhibition/variable slopes" equation that was performed using GraphPad Prism version 5.00 for Windows (GraphPad Software, San Diego CA, www.graphpad.com). The experimental data are representative example of three independent experiments. In most cases, the standard deviations were almost within 5% of the experimental values, except for some inhibition data points where standard errors of means were within 10% of the measured values. $p < .05$ was considered statistically significant.

### Determination of the inhibition mode and constants

To determination of inhibition mode, the Michaelis–Menten constant ($K_m$) and maximum velocity ($V_{max}$) and inhibition constants ($K_i$ and $K_I$) values were obtained using Equation (1)[29,30] in the presence of at least four concentrations of each compound which were selected from concentration–activity curves. The data were analyzed by nonlinear regression using the program GraphPad Prism

$$v = \frac{V_{max}[S]}{[S](1 + [I]/K_i) + K_m(1 + [I]/K_i)}, \quad (1)$$

where $K_i$ and $K_I$ are the equilibrium dissociation constants for competitive and uncompetitive inhibitor binding, respectively, while, *v*, [S] and [I] represent the rate of product formation, the substrate and the inhibitor concentration, respectively[29]. It has been found that there are two inhibitor constants: $K_i$, which defined as the dissociation constant of the enzyme–inhibitor complex, and $K_I$, which defined as the dissociation constant of the enzyme–substrate–inhibitor complex. If $K_i < K_I$, the type of enzyme inhibition was defined as competitive-noncompetitive and if $K_i > K_I$, the type of enzyme inhibition was defined as uncompetitive–noncompetitive. The type of enzyme inhibition was defined as pure noncompetitive inhibition when $K_i = K_I$[30–32]. For better visual presentation of data of inhibition mode, the Lineweaver–Burk plots were also provided.

### Docking studies

The structures of molecules were drawn and optimized using HyperChem (HyperCube Inc., Gainesville, FL). Semi-empirical AM1 method with Polak–Ribiere algorithm until the root mean square gradient of 0.01 kcal $mol^{-1}$ was used as the optimization method. The crystal structure of rkbPAP retrieved from the Protein Data Bank (PDB code: 2QFR) was used. Then, after determining Kollman united atom charges[33] and merging nonpolar hydrogens, rotatable bonds were assigned. Using autoGrid tool, the grid maps (one for each atom type in the ligand, and one for electrostatic interactions) were constructed adequately large to include the active site of enzyme as well as significant regions of the surrounding

surface. In all the cases, a grid map of 60 points in each Cartesian direction besides a grid-point spacing of 0.375 Å (a quarter of the carbon–carbon single bond) were generated. By the ligand location in the complex of ligand–enzyme, the maps were centered on the binding site (Zn atom of the enzyme), searching effective interactions with the functional groups. Based on Lamarckian Genetic Algorithm[34], using the pseudo-Solis and Wets local search method[35], AutoDock Tools was employed to produce both grid and docking parameter files, that is .gpf and .dpf files. Applying 0.5 Å clustering tolerance to construct clusters of the closest compounds, the initial coordinates of the ligand were used as the reference structure. Finally, docking results (enzyme–inhibitor complex) were visualized using Viewer Lite 4.2.

## Results and discussion

### Chemistry

The conversion of 4-methoxybenzaldehyde (**1**) into diethyl (amino(4-metoxybenzyl)-methyl)phosphonate was achieved by heating **1** with a mixture of ammonium acetate and diethyl phosphite over activated molecular sieves in ethanol, according to a literature procedure reported for the synthesis of diethyl α-aminobenzylphosphonate from benzaldehyde (Scheme 1)[36]. Introducing hydrogen chloride gas to the free amine product gave its corresponding hydrochloride salt **2** in 23% overall yield[36]. Alkylation of **2** to give the sulfonamides **3a**–**d** was achieved with adding appropriate sulfonyl chlorides and DIPEA to **2** in chloroform. The reaction mixture was stirred under nitrogen atmosphere for 24 h. The final synthetic step to produce the newly designed inhibitors **4a**–**d** required the cleavage of the phosphonate ester bonds of **3a**–**d** to give their corresponding free phosphonic acids. This was achieved by stirring **3a**–**d** with a mixture of potassium iodide and trimethylsilyl chloride in chloroform at 25 °C for 24 h that giving the desired products in moderate yields.

### Enzyme purification and biological activity measurements

Although human PAP (hPAP) would be the best choice for our purposes, hPAP can only be obtained in minute quantities using a baculoviral recombinant expression system[37]. However, as stated earlier, rkbPAP is a valid model of hPAP (see Figure 1), as indicated by the highly conserved active sites across these different enzymes, the similarities in substrate binding pockets, and the similarities of inhibition constants for a range of structurally different inhibitors reported for several animal (including human) and plant PAPs[18,26]. The rkbPAP was purified from red kidney bean according to the method described by Beck et al.[8] The SDS–PAGE analysis is shown in Figure 1, which clearly indicates the reasonable purity of the isolated PAP. The densitometry of bands indicates that the mass fraction of the purified enzyme is around 0.90 (∼90% purity). It is noteworthy that the plant enzymes are mostly dimeric glycoproteins, and have subunit molecular masses of 50–60 kD. As shown in the figure, differential glycosylation of the subunits, leading to a heterogeneity in the molecular mass of the subunits, has been reported for kidney bean PAP, which is a dimeric glycoprotein (molecular mass 110 kD) with an inter-subunit disulfide linkage[11]. Activity staining on PAGE gel also showed that only the ∼50 kDa bands had esterase activity, confirming that there is no contaminant phosphatase enzymes other than desired PAP (data not shown).

The isolated rkbPAP was assayed using *p*-NPP as a substrate. The obtained $K_m$ and $V_{max}$ by fitting data to the Michaelis–Menten equation were 12.6 ± 1.4 and 48 ± 6, respectively. We also designed/synthesized and evaluated the catalytic effects of a number of new inhibitor candidates of rkbPAP, based on the alkylsulfonamido(4-methoxyphenyl)methyl)phosphonic acid scaffold. The inhibitory effects of derivatives **3a**–**d** and **4a**–**d** as well as tartrate as the positive control were tested against rkbPAP at pH 4.9[38]. In order to identifying the PAP inhibition mode of test compounds and determining apparent kinetic parameters, the kinetic data were analyzed using Equation (1). The $IC_{50}$ and inhibition constant ($K_i$ and $K_I$) values of test compounds have been summarized in Table 1. As it was expected, PAP activity was weakly inhibited by tartrate, which is in good agreement with previous reports[11,38–40]. Most of the synthesized compounds demonstrated their inhibitory potentials on PAP in a dose-dependent manner.

**Table 1.** Kinetic data for inhibitors against rkbPAP at pH 4.9.

| Inhibitor name | $IC_{50}$ (μM) | $K_i$ (μM) | $K_I$ (μM) |
|---|---|---|---|
| **3a** and **3b** | Very weak inhibitor | – | – |
| **3c** | 759 | 202 ± 11 | 211 ± 8 |
| **3d** | 92 | 13 ± 1 | 36 ± 3 |
| **4a** and **4b** | Very weak inhibitor | – | – |
| **4c** | 421 | 95 ± 9 | 103 ± 5 |
| **4d** | 13 | 1.1 ± 0.2 | 8.2 ± 1.4 |
| Tartrate | 3315 | 783 ± 41 | – |

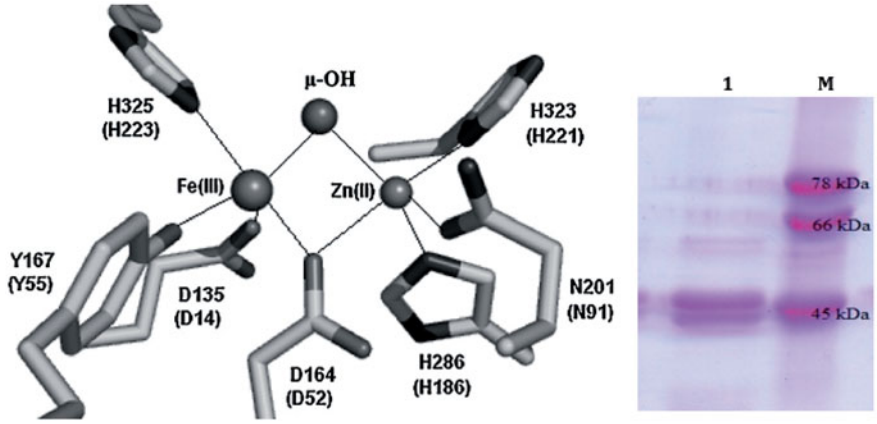


**Figure 1.** (Left) Active site of all known PAPs has an $Fe^{3+}$ in the active site, which coordinates with an invariant tyrosine ligand, producing a ligand to metal CT transition giving rise to the characteristic purple color of the enzyme. PAPs active site also contains a divalent metal ion which may be either $Zn^{2+}$, $Mn^{2+}$ or $Fe^{2+}$. The seven metal ion-coordinating residues are invariant among PAPs from different sources. Residue labels refer to the sequences of red kidney bean PAP and pig PAP (in brackets or parentheses). Taken from Schenk et al.[5] (Right) SDS–PAGE illustrates PAP purity (lane 1). M, molecular size markers.

Among the evaluated compounds, **3d** ($IC_{50} = 92\,\mu M$, $K_i = 13 \pm 1\,\mu M$), **4c** ($IC_{50} = 421\,\mu M$, $K_i = 95 \pm 9\,\mu M$) and **4d** ($IC_{50} = 13\,\mu M$, $K_i = 1.1 \pm 0.2\,\mu M$), were the most potent inhibitors; of which **3d** and **4d** were recognized as potent inhibitors of PAP even stronger than the standard inhibitor[11,38–40]. As can be seen, the $K_i$ values are in reasonable agreement with the $IC_{50}$ values, comparable at least with the best of the naphthalenemethylphosphonic acid derivatives[3,18]. Also, the **3a**, **3b**, **4a** and **4b** exhibited negligible inhibitions of PAP, in millimolar range. Thus, these compounds were excluded from further studies (determination of inhibition mode).

Although an in depth SAR analysis is currently impossible, it appears that a major improve in rkbPAP inhibitory activity correlates with increasing the asymmetric hydrophobicity of the compounds. It appears that inhibitor potency increases with increase the length of alkyl chain in alkylsulfonamide moieties (Table 1 and Scheme 1), so that the largest effect on inhibition was achieved with the hexadecyl moiety. Substitution at the dodecyl (in **3c**/**4c**) with hexadecyl (in **3d**/**4d**) greatly decrease the inhibition constant of the inhibitor, suggesting an extremely large hydrophobic or sterically tolerant region near/not into the phosphate binding site of the enzyme as well as a possible preference for the long-chain acyl ($\geq C_{12}$) derivatives. McGeary et al. was reported a similar trend for the rkbPAP and pig PAP enzymes, that is, the longer the alkyl chain the more potent inhibitor of PAPs[18].

The inhibition modes of the compounds can be elicited by comparing values of $K_i$ and $K_I$ and represented by Lineweaver–Burke plot. Typical Lineweaver–Burk plots for inhibitory activity of **3c** and **4d** as representative have been demonstrated in Figure 2. If the Lineweaver–Burke plot shows crisscross lines at a single point on the $1/V$ ($y$) axis, it is indicative of competitive inhibition. Also, the trend lines of Lineweaver–Burke plot for **3c** and **4c** compounds intersect each other on the $1/S$ ($x$) axis, which is characteristic of noncompetitive inhibition, so $K_i \approx K_I$. Such noncompetitive mode inhibition has also been previously reported for hexyl-derivative of α-alkoxynaphthylmethylphosphonic acid[18]. For longer chain-length inhibitors (**3d** and **4d**), the lines of the Lineweaver–Burke plot intersect at a single point between $x$- and $y$-axis, close to the $1/S$ axis, indicate that PAP activity was inhibited with mixed manner by these compounds. On the other hand, since $K_i < K_I$, the exact mechanism of inhibition is competitive–noncompetitive[18,23,26,31]. In agreement with this mode change, McGeary et al. reported that longer alkyl chains of α-alkoxynaphthylmethylphosphonic acid derivatives inhibit rkbPAP and pPAP with mixed (competitive–noncompetitive) manner[18]. This behavior may reflect a stronger anchoring effect of the longer alkyl chains into the groove adjacent to the active site of the enzyme, which would favor partially competitive inhibition. Furthermore, the replacement of the diethyl phosphonate group of series **3** by phosphonate in series **4** has a minor decrement effect on the inhibitory effect of compound and does not alter the mode of inhibition, since probably this moiety is not bind/coordinate to bimetal/binuclear center.

### *Molecular docking studies*

Molecular docking studies on binding modes are essential to elucidate key structural characteristics and interactions and they provide helpful data for designing effective PAP inhibitors[41]. Hence, to make the rational design of novel and more selective PAP inhibitors possible, molecular docking was carried out on PAP binding pocket using a set of PAP inhibitors shown in Scheme 1. As well as RMSD cluster analysis, AutoDock also uses binding free energy assessment to assign the best binding conformation. Energies estimated by AutoDock are described by intermolecular energy (including van der Waals, hydrogen bonding, desolvation,

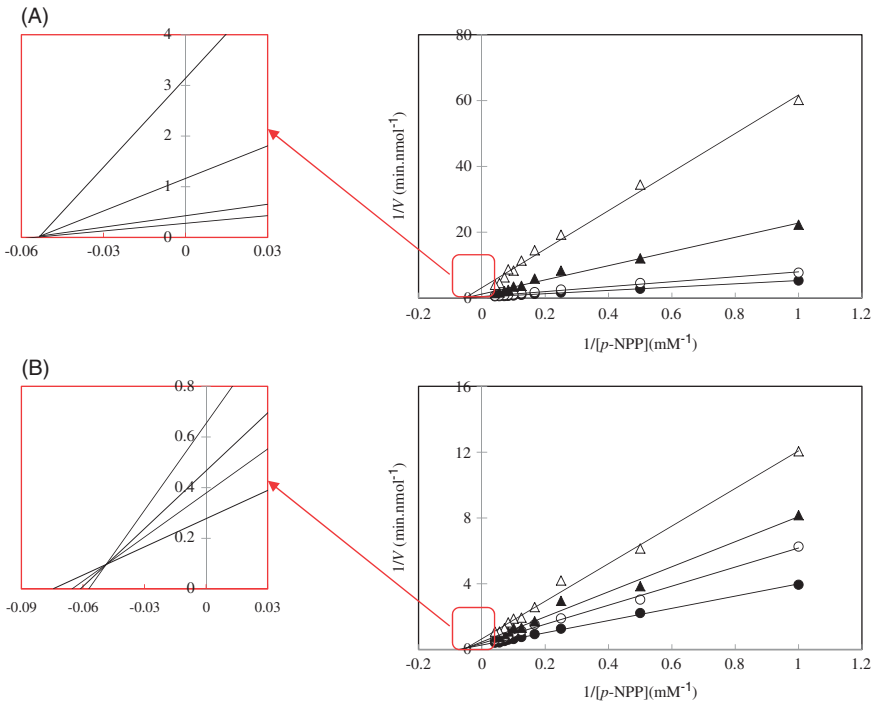


**Figure 2.** Typical Lineweaver–Burk plots for inhibitory activity of synthetic compounds against rkbPAP. The data represent the average of 3–5 experiments. (A) Lineweaver–Burk plot of rkbPAP activity in the absence (•) and the presence of 300 (○), 600 (▲) and 1200 μM of **3c** (△). (B) Lineweaver–Burk plot of rkbPAP activity in the absence (·) and the presence of 10 (○), 20 (▲) and 40 μM of **4d** (△).

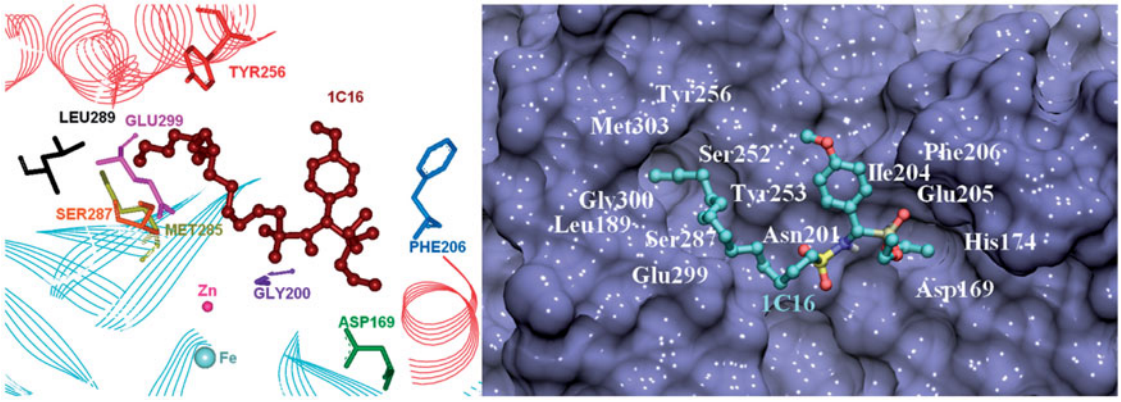


**Figure 3.** The three-dimensional representation of docking result of **3d** in the close vicinity of rkbPAP binding pocket (left). Surface and stick representation of the predicted binding mode of **3d** to the enzyme based on docking simulations (right).

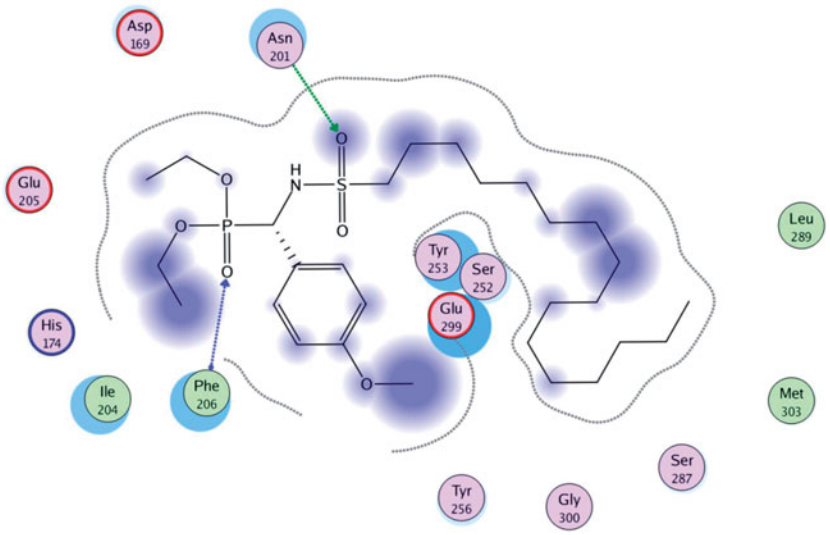


**Figure 4.** The two-dimensional representation of docking result of **3d** compound with binding pocket of rkbPAP.

and electrostatic energies), internal energy, and torsional free energy[42]. Among these calculated energies by AutoDock, the first two provide the docking energy, while the sum of the first and the third items account for the binding energy. Among all interactions occurring in the active site, the electrostatic interaction between the ligand and the enzyme is the most significant, because in most cases it can assign the strength of binding and the exact position of the inhibitor in the binding site energy[42].

The docking results show that all of the studied compounds occupy an almost similar space in the binding site. Also, the calculated binding affinities using computational modeling correlate well with measured inhibition constants (results not shown). Unexpectedly, modeling suggests that the phosphonate moiety of the **3d** inhibitor does not bind to the dimetal center in the active site of rkbPAP. Furthermore, the alkyl chain of the inhibitor binds to the groove on the surface of the enzyme. Other part of molecules including polar atoms and aromatic portions are placed on the hydrophilic patch around the active site, which is in good agreement with the obtained inhibition modes. The best possible binding mode of **3d** as the most biologically active compound in the rkbPAP binding site is illustrated in a three-dimensional (Figure 3) and two-dimensional space (Figure 4).

On the other hand, to obtain a detailed description of the effects of individual residues on binding affinity, a per-residue decomposition of the total energy was carried out to evaluate the energetic influences of critical residues on the binding. The residues were separately studied, and the Van der Waals, electrostatic and interaction energies of these residues and **3d** were determined. These include Phe-206, Glu-299, Gly-200, Asp-169, Tyr-256, Ser-287, Met-285 and Leu-289 (Table 2). Energy of interaction between individual residues and ligand was calculated with the "Calculate Interaction Energy" protocol encoded in Discovery Studio. The complexes were typed with CHARMM force field. All parameters used were kept at their default settings. The residue-based decomposition of interaction energies identified several critical residues of PAP. Table 2 lists the calculated energies contributions of these key residues of interest. As can be seen, major favorable energy contributions originate predominantly from Phe-206 and Glu-299. The methoxy phenyl core of **3d** is anchored by

**Table 2.** Interaction, van der Waals and electrostatic energies for selected residues of PAP and **3d**.

| Residue | Interaction energy (kcal/mol) | VDW interaction energy (kcal/mol) | Electrostatic interaction energy (kcal/mol) |
|---|---|---|---|
| PHE206 | −12.1 | −3.78 | −8.30 |
| GLU299 | −11.3 | −3.86 | −7.47 |
| GLY200 | −7.45 | −0.18 | −7.27 |
| ASP169 | −7.32 | 0.02 | −7.35 |
| TYR256 | −3.67 | −1.66 | −2.01 |
| SER287 | −2.60 | 15.2 | −17.8 |
| MET285 | −1.22 | −0.62 | −0.60 |
| LEU289 | −0.27 | −0.27 | 0.0 |

an aromatic stacking interaction with Phe-206, whereas Glu-299 is one of major contributor of van der Waals interactions.

As it can be concluded from Figures 3, 4 and Table 2, the major part of the binding cavity of rkbPAP is hydrophilic, which allows for the tight binding of polar substrates and inhibitors. A long apolar groove adjacent to the active site was identified as an additional potential point of interaction of hydrophobic aliphatic chain and is required for recognition and directionality of the substrate aliphatic chain functionality[18]. Also, hydrogens of $NH_2$ group of Asn-201 side chain and sulfonamide group of ligand, also hydrogens of $NH_2$ group of Phe-206 backbone and oxygen of phosphonate group of ligand form hydrogen bonds (3.12 and 2.90 Å, respectively). It is was interesting to note that the aliphatic chain orients inside the binding cavity and interacts by both hydrophobic as well as hydrophilic interactions (Table 2) with amino acids such as Leu-289 and Met-303. With respect to the docking results (Figures 3 and 4) Ser-252, Tyr-256, Ser-287, Met-303 and Leu-289 assemble one hydrophobic cluster, which accommodates the aliphatic hydrophobic chain moiety of the ligand. Taking literature[26] into account, similar binding orientations of inhibitors in the active sites of pig, red kidney bean and hPAP, may support the contention that the inhibitory potencies obtained using rkbPAP can be extrapolated to hPAP.

## Conclusions

To the best of our knowledge, there are no published reports in the literature on the application of alkylsulfonamidophenyl)methyl)phosphonic acid derivatives as potential PAP inhibitors. In the current work, we identified these new derivatives of alkylsulfonamido(4-methoxyphenyl)methyl)phosphonic acid, as potent inhibitors of rkbPAP. The hexadecyl derivative (4d, with $K_i$ value of 1.1 μM) was found to be the most active compared to compounds contain shorter alkyl chains. In addition, it was illustrated that the inhibitor bound in the vicinity of the enzyme active site showed mixed mode inhibition due to partial competition whit substrate. Considering the crucial role(s) of mammalian PAPs in bone metabolism, such inhibitors are anticipated to be promising lead compounds in the development of new anti-osteoporotic chemotherapeutics.

## Acknowledgement

This work was performed in partial fulfillment of the requirements for Pharm. D. of N. Alimoradi, in Faculty of Pharmacy, Kermanshah University of Medical Sciences, Kermanshah, Iran.

## Disclosure statement

The authors declare that they have no conflict of interests.

## Funding

The financial support [Grant No. 92047] from the Research Council of Kermanshah University of Medical Sciences is gratefully acknowledged.

## References

1. Mitić N, Smith SJ, Neves A, et al. The catalytic mechanisms of binuclear metallohydrolases. Chem Rev 2006;106:3338–63.
2. Oddie G, Schenk G, Angel N, et al. Structure, function, and regulation of tartrate-resistant acid phosphatase. Bone 2000;27:575–84.
3. Schwender CF, Beers SA, Malloy E, et al. 1-naphthylmethylphosphonic acid derivatives as osteoclastic acid phosphatase inhibitors. Bioorg Med Chem Lett 1995;5:1801–6.
4. Hayman AR, Jones SJ, Boyde A, et al. Mice lacking tartrate-resistant acid phosphatase (Acp 5) have disrupted endochondral ossification and mild osteopetrosis. Development 1996;122:3151–62.
5. Schenk G, Mitić N, Hanson GR, Comba P. Purple acid phosphatase: a journey into the function and mechanism of a colorful enzyme. Coord Chem Rev 2013;257:473–82.
6. Bernhardt PV, Schenk G, Wilson GJ. Direct electrochemistry of porcine purple acid phosphatase (uteroferrin). Biochemistry 2004;43:10387–92.
7. Wang DL, Holz RC, David SS, et al. Electrochemical properties of the diiron core of uteroferrin and its anion complexes. Biochemistry 1991;30:8187–94.
8. Beck JL, McConachie LA, Summors AC, et al. Properties of a purple phosphatase from red kidney bean: a zinc-iron metalloenzyme. BBA-Protein Struct M 1986;869:61–8.
9. Leung EW, Teixeira M, Guddat LW, et al. Structure, function and diversity of plant purple acid phosphatases. Curr Topic Plant Biol 2007;8:21–31.
10. Schenk G, Guddat L, Ge Y, et al. Identification of mammalian-like purple acid phosphatases in a wide range of plants. Gene 2000;250:117–25.
11. Cashikar AG, Kumaresan R, Rao NM. Biochemical characterization and subcellular localization of the red kidney bean purple acid phosphatase. Plant Physiol 1997;114:907–15.
12. Nuttleman PR, Roberts RM. Transfer of iron from uteroferrin (purple acid phosphatase) to transferrin related to acid phosphatase activity. J Biol Chem 1990;265:12192–9.
13. Sibille J-C, Doi K, Aisen P. Hydroxyl radical formation and iron-binding proteins. Stimulation by the purple acid phosphatases. J Biol Chem 1987;262:59–62.
14. Räisänen SR, Alatalo SL, Ylipahkala H, et al. Macrophages overexpressing tartrate-resistant acid phosphatase show altered profile of free radical production and enhanced capacity of bacterial killing. Biochem Biophys Res Commun 2005;331:120–6.
15. Boonen S. Bisphosphonate efficacy and clinical trials for postmenopausal osteoporosis: similarities and differences. Bone 2007;40:S26–31.
16. Halleen JM, Tiitinen SL, Ylipahkala H, et al. Tartrate-resistant acid phosphatase 5b (TRACP 5b) as a marker of bone resorption. Clin Lab 2006;52:499–510.
17. Vella P, McGeary RP, Gahan LR, Schenk G. Tartrate-resistant acid phosphatase: a target for anti-osteoporotic chemotherapeutics. Curr Enzyme Inhib 2010;6:118–29.
18. McGeary RP, Vella P, Mak JY, et al. Inhibition of purple acid phosphatase with alpha-alkoxynaphthylmethylphosphonic acids. Bioorg Med Chem Lett 2009;19:163–6.
19. Susi F, Goldhaber P, Jennings JM. Histochemical and biochemical study of acid phosphatase in resorbing bone in culture. Am J Physiol 1966;211:959–62.
20. Angel NZ, Walsh N, Forwood MR, et al. Transgenic mice overexpressing tartrate-resistant acid phosphatase exhibit an increased rate of bone turnover. J Bone Miner Res 2000;15:103–10.
21. Valizadeh M, Schenk G, Nash K, et al. Phosphotyrosyl peptides and analogues as substrates and inhibitors of purple acid phosphatases. Arch Biochem Biophys 2004;424:154–62.

22. Reszka AA, Rodan GA. Bisphosphonate mechanism of action. Curr Rheumatol Rep 2003;5:65–74.
23. Pinkse MW, Merkx M, Averill BA. Fluoride inhibition of bovine spleen purple acid phosphatase: characterization of a ternary enzyme–phosphate–fluoride complex as a model for the active enzyme–substrate–hydroxide complex. Biochemistry 1999;38:9926–36.
24. Crans DC, Simone CM, Holz RC, Que L Jr. Interaction of porcine uterine fluid purple acid phosphatase with vanadate and vanadyl cation. Biochemistry 1992;31:11731–9.
25. Myers JK, Antonelli SM, Widlanski TS. Motifs for metallophosphatase inhibition. J Am Chem Soc 1997;119:3163–4.
26. Mohd-Pahmi SH, Hussein WM, Schenk G, McGeary RP. Synthesis, modelling and kinetic assays of potent inhibitors of purple acid phosphatase. Bioorg Med Chem Lett 2011;21:3092–4.
27. Kaboudin B, Rahmani A. Convenient synthesis of 1-aminoalkylphosphonates under solvent-free conditions. Org Prep Proced Int 2004;36:82–6.
28. Lowry OH, Rosebrough NJ, Farr AL, Randall RJ. Protein measurement with the Folin phenol reagent. J Biol Chem 1951;193:265–75.
29. Feder D, Hussein WM, Clayton DJ, et al. Identification of purple acid phosphatase inhibitors by fragment-based screening: promising new leads for osteoporosis therapeutics. Chem Biol Drug Des 2012;80:665–74.
30. Choughule KV, Barr JT, Jones JP. Evaluation of rhesus monkey and guinea pig hepatic cytosol fractions as models for human aldehyde oxidase. Drug Metab Dispos 2013;41:1852–8.
31. Siah M, Farzaei MH, Ashrafi-Kooshk MR, et al. Inhibition of guinea pig aldehyde oxidase activity by different flavonoid compounds: an *in vitro* study. Bioorg Chem 2016;64:74–84.
32. Pirouzpanah S, Rashidi MR, Delazar A, et al. Inhibitory effects of *Ruta graveolens* L. extract on guinea pig liver aldehyde oxidase. Chem Pharm Bull 2006;54:9–13.
33. Weiner SJ, Kollman PA, Case DA, et al. A new force field for molecular mechanical simulation of nucleic acids and proteins. J Am Chem Soc 1984;106:765–84.
34. Morris GM, Goodsell DS, Halliday RS, et al. Automated docking using a Lamarckian genetic algorithm and an empirical binding free energy function. J Comput Chem 1998;19:1639–62.
35. Solis FJ, Wets RJB. Minimization by random search techniques. Math Oper Res 1981;6:19–30.
36. Hua F, Meijuan F, Xiaoxia L, et al. Syntheses, characterizations, and crystal structures of phosphonopeptides. Heteroat Chem 2007;18:9–15.
37. Marshall K, Nash K, Haussman G, et al. Recombinant human and mouse purple acid phosphatases: expression and characterization. Arch Biochem Biophys 1997;345:230–6.
38. Kilsheimer GS, Axelrod B. Inhibition of prostatic acid phosphatase by alpha-hydroxycarboxylic acids. J Biol Chem 1957;227:879–90.
39. Siddiqua A, Saeed A, Naz R, et al. Purification and biochemical properties of acid phosphatase from Rohu fish liver. Int J Agric Biol 2012;14:223–8.
40. Kaida R, Hayashi T, Kaneko TS. Purple acid phosphatase in the walls of tobacco cells. Phytochemistry 2008;69:2546–51.
41. Lisina K, Piramanayagam S. An *in silico* study on HIV-1 protease wild-type and mutant with inhibitors from Annona squamosa. Int J Pharm Sci Res 2014;5:1811–18.
42. Shahlaei M, Madadkar-Sobhani A, Mahnam K, et al. Homology modeling of human CCR5 and analysis of its binding properties through molecular docking and molecular dynamics simulation. Biochim Biophys Acta 2011;1808:802–17.